Available online at www.sciencedirect.com

SCIENCE DIRECT

Biochimica et Biophysica Acta 1707 (2005) 103–116

BIOCHIMICA ET BIOPHYSICA ACTA
BBA

http://www.elsevier.com/locate/bba

Review

Exploring amino-acid radical chemistry: protein engineering and de novo design

Kristina Westerlund, Bruce W. Berry, Heidi K. Privett, Cecilia Tommos*

Department of Biochemistry and Biophysics, Arrhenius Laboratories for Natural Sciences, Stockholm University, SE-106 91 Stockholm, Sweden

Received 17 July 2003; accepted 26 February 2004
Available online 6 May 2004

Abstract

Amino-acid radical enzymes are often highly complex structures containing multiple protein subunits and cofactors. These properties have in many cases hampered the detailed characterization of their amino-acid redox cofactors. To address this problem, a range of approaches has recently been developed in which a common strategy is to reduce the complexity of the radical-containing system. This work will be reviewed and it includes the light-induced generation of aromatic radicals in small-molecule and peptide systems. Natural redox proteins, including the blue copper protein azurin and a bacterial photosynthetic reaction center, have been engineered to introduce amino-acid radical chemistry. The redesign strategies to achieve this remarkable change in the properties of these proteins will be described. An additional approach to gain insights into the properties of amino-acid radicals is to synthesize de novo designed model proteins in which the redox chemistry of these species can be studied. Here we describe the design, synthesis and characteristics of monomeric three-helix bundle and four-helix bundle proteins designed to study the redox chemistry of tryptophan and tyrosine. This work demonstrates that de novo protein design combined with structural, electrochemical and quantum chemical analyses can provide detailed information on how the protein matrix tunes the thermodynamic properties of tryptophan.

Keywords: De novo protein design; Maquette; Protein radical; Tyrosyl radical; Tryptophanyl radical; Redox-active amino acid

1. Introduction

The role of amino-acid radicals in biological electron transfer and proton-coupled electron transfer continues to excite both experimental [1] and theoretical interest [2]. The characterization of amino-acid redox cofactors in natural proteins can be challenging for several reasons. The sheer size and complexity of many amino-acid radical enzymes, combined with the often highly oxidizing nature of their radical cofactors, hampers electrochemical and spectroscopic measurements. Other cofactors, non-catalytically active amino acids, or even the solvent, may be oxidized before the residue of interest and/or their spectra obscure the weak spectral features of amino-acid radicals (ε_{max}<3000 M^{-1} cm^{-1}; Refs. [3–5]). To address some of these issues, a range of approaches has been developed in which a common strategy is to reduce the complexity of the radical-containing system. These approaches include the light-induced generation of aromatic radicals in small-molecule and peptide systems, the redesign of structurally well-characterized natural enzymes to introduce amino-acid radical function, and the synthesis of de novo designed radical proteins. Here we review the structural and functional characteristics of small-molecule and peptide/protein model systems that have been constructed to investigate amino-acid redox chemistry. To provide a background to the synthetic and protein engineering and design work, we start by briefly summarizing the biological reactions catalyzed by amino-acid radical enzymes and highlight some of the fascinating properties of these systems.

1.1. Amino-acid radical enzymes

Four amino acids—tyrosine, tryptophan, cysteine and glycine—have been shown to form catalytically active, one-electron oxidized radicals [1]. The family of enzymes

* Corresponding author. Tel.: +46-8-162446; fax: +46-8-153679.
E-mail address: cecilia@dbb.su.se (C. Tommos).

0005-2728/$ - see front matter © 2004 Elsevier B.V. All rights reserved.
doi:10.1016/j.bbabio.2004.02.013

that contains amino-acid based radical cofactors are involved in a broad range of biochemical processes [1,2] including, for example, carbohydrate metabolism. The catalytic cycle of pyruvate formate lyase involves both glycyl and cysteinyl radicals [6,7] and a redox-active tyrosinate is present in the active sites of galactose oxidase and glyoxal oxidase [8]. The ribonucleotide reductase enzymes utilize three, if not all four, of the amino-acid redox cofactors in the conversion of ribonucleotides to deoxyribonucleotides [9–11]. The chemical reactions that give rise to radicals in these enzymes are remarkably diverse and divide the ribonucleotide reductases into three major classes. The class I enzymes employ O_2-dependent chemistry at a di-iron center to generate the driving force necessary to oxidize a tyrosine adjacent to the metal site. The class II enzymes utilize an adenosylcobalamin cofactor to trigger formation of a transient carbon radical. Finally, the glycyl radical required for the activity of the class III ribonucleotide reductases is formed via an iron-sulfur cluster/*S*-adenosylmethionine dependent redox process. The common function of these metallo-radical cofactors is to oxidize a cysteine located at the active site. Once formed, the transient thiyl radical initiates catalysis by abstracting a hydrogen atom from the 3′position of the substrate ribose unit. As will be described here, efforts have been made to develop light-dependent methods to artificially drive electron/proton transfers in the class I enzymes [12].

In addition to playing a central role in nucleic acid biosynthesis, Aubert et al. [13,14] have recently shown that amino-acid redox cofactors are involved in DNA repair. DNA photolyase harvests light in the blue or near-ultraviolet region of the electromagnetic spectrum and uses the photon energy to repair UV-light damaged DNA [15]. A chain of three redox-active tryptophans has been detected in the *Escherichia coli* enzyme [13] and both oxidized tryptophan and tyrosine residues have been found in the corresponding enzyme from *Anacystis nidulans* [14]. Aromatic amino acids also serve as essential redox mediators in several heme-containing peroxidases. The compound I state of cytochrome *c* peroxidase involves a heme oxyferryl species and a tryptophanyl cation radical [16] whereas the peroxidase activity of prostaglandin H synthase requires the participation of a tyrosyl radical [17]. In addition, the catalytic cycles of bovine liver catalase [18] and lioneate diol synthase [19] have also been suggested to involve tyrosyl radicals. In order to catalyze this variety of chemical reactions, the protein environment tunes the redox properties of the radical cofactor. For example, the reduction potential of the tryptophanyl cation radical in cytochrome *c* peroxidase is lowered by local electronegative interactions [20]. In this review, we will describe a study in which de novo protein design was combined with quantum chemical methods to investigate the effects of a charge-π interaction on the thermodynamic properties of tryptophan [21].

Tyrosine redox chemistry is involved in energy transduction in photosynthesis and respiration. Studies performed in the late 1980s showed that photosystem II contains two redox-active tyrosines, denoted Y_Z and Y_D, of which the former is essential for the unique water-splitting reactions catalyzed by this enzyme [22]. More recent data have indicated that the cross-linked histidine-tyrosine residue located at the active site of cytochrome *c* oxidase forms a radical during the catalytic cycle [23]. Mechanistic models for photosystem II [2,24–27] and cytochrome *c* oxidase [2,23,28–30], as well as for the class I ribonucleotide reductases [2,9–12], involve the participation of tyrosine in both electron and proton transfers. The role of tyrosine as a proton coupled electron-transfer cofactor is a topic that has attracted a lot of attention, and accordingly, represents a focal point of several of the studies described below.

The free energy that fuels the catalytic cycles in amino-acid radical enzymes originates either from light or from redox potential energy. These proteins contain an inducible oxidant, which upon activation extracts an electron from a nearby amino acid thereby creating the radical that is capable of such remarkably diverse chemistry. The oxidant can be of organic origin, a metal, or a combination of both. For example, a photooxidized chlorophyll radical serves as the amino-acid radical generator in photosystem II and a photoexcited FADH semiquinone triggers tryptophan oxidation in DNA photolyase. Other proteins utilize metal-based redox chemistry to trigger radical formation, as illustrated for example by the class I ribonucleotides reductases and the heme peroxidases described above. Formation of the glycyl radicals in the anaerobic pyruvate formate lyase and class III ribonucleotide reductase enzymes requires $[Fe_4S_4]^{+1}$-containing activases [31]. The proposed function of the activase is to reduce *S*-adenosylmethionine. The radical fragment produced by the reductive bond-cleavage event, in turn, abstracts a hydrogen atom from the active site glycine.

Although the oxidant and the radical species differ in the various systems, amino-acid radical enzymes have several common properties. One characteristic is that these enzymes typically operate at highly oxidizing potentials [1,2]. Despite this, several of the amino-acid radicals are remarkably stable (e.g. Refs. [8,9,16,22]). The control the protein matrix has over the radical is also illustrated in the redox reversibility of catalytic protein radicals relative to the properties of these species in solution. For example, tyrosine oxidation is an irreversible process in solution [32]. In contrast, the redox cycles of Y_Z and Y_D are reversible with the former being oxidized and reduced about 200 times per second in saturating light [33]. Another evidence of strict control is provided by the fact that some enzymes, e.g. prostaglandin H synthase and photosystem II, generate and confine the amino-acid radical at the active site. In other systems, such as the class I ribonucleotide reductases and DNA photolyase, long-range radical migration readily occurs. The apparent ease by which the proteins handle their highly reactive cofactors is impressive and suggests that these

enzymes have evolved mechanisms to thermodynamically and/or kinetically stabilize the generated radical, avoid unwanted side reactions, and direct the reactive species at the substrate. The work reviewed here is aimed at gaining insights into these mechanisms.

2. Radical generation and characterization in model systems

Electron-transfer rates are influenced by the temperature, the driving force of the reaction (ΔG°), the nuclear reorganization energy (λ) and the electronic coupling between the donor (D) and acceptor (A) molecules [12,34]. The reorganization energy reflects the change in structure of the redox cofactors and the surrounding medium necessary to permit electron transfer from D to A. The interplay between ΔG° and λ determines the height of the energy barrier for the electron-transfer. The electron coupling term formally depends exponentially on the D–A distance and on the properties of the intervening medium. A central issue in the consideration of biological electron transfer mediated by proteins is whether evolution has selected structural properties or features on the basis of the detailed pathway(s) of electron transfer or on the basis of more generic properties such as the distance between D–A pairs and the packing density and basic nature of the intervening medium (for reviews, see Refs. [35–37]). Additional points of controversy include details about how the D–A distance should be characterized (i.e., edge-to-edge vs. center-to-center of the participating moieties), the consideration of dynamics, and the maximal magnitude of an endergonic tunneling step between two sites in a chain of redox cofactors participating in an overall exergonic electron-transfer reaction.

The elegant studies performed to elucidate electron tunneling in proteins have involved work on many different types of redox cofactors but, to date, very few investigations have been done in which amino-acid radicals are involved in the process. In order to gain more insights into the properties of these cofactors, various approaches to induce and characterize amino-acid radical reactions have recently been reported in the literature. A common theme of this work is that radical formation is triggered with light and it includes studies on small-molecule and peptide systems as well as protein engineering.

2.1. Small-molecule systems

Photoactive ruthenium complexes have been used extensively to investigate the dependence of driving force, distance and pathway on the rate of electron tunneling between protein redox cofactors [35,38]. A number of protocols have been developed to append ruthenium polypyridyl compounds to histidine, lysine or cysteine residues located on the protein surface and to trigger the electron-transfer reactions by a laser flash (see Ref. [38] and references therein). Of particular interest here is the bimolecular laser flash-quench technique developed by Bjerrum et al. [39] in which the long-lived, photo-excited Ru(II)* state is efficiently converted into Ru(III) by an externally added sacrificial oxidant. With an appropriate choice of ligands, the reduction potential of the Ru(III)/Ru(II) redox couple can be made sufficiently oxidizing to generate amino-acid radicals. Magnuson et al. [40] took advantage of these properties of the ruthenium-based photosensitizers in the construction of a biomimetic model system for the water-oxidation complex of photosystem II. In the photosystem II reaction center, a multimeric chlorophyll complex denoted P_{680} forms upon light absorption a highly oxidizing cation radical. This chlorophyll species oxidizes the nearby Y_Z tyrosine, which in turn, is reduced by the substrate–water binding manganese cluster [24]. In the biomimetic system constructed by the Swedish groups, the photoactive P_{680} species and the Y_Z radical cofactor are modeled by a Ru(II) tris-bipyridyl complex with a covalently attached tyrosine residue (see Fig. 1). In an initial study of this complex, it was shown that the light-excited Ru(II)* complex could be oxidized to Ru(III) on the nanosecond time scale using the laser flash-quench technique [40]. The photo-oxidation event was followed by intramolecular electron transfer from the tyrosine to the metal resulting in the regeneration of the Ru(II) state and the formation of a tyrosyl radical. The observed radical is neutral and thus the tyrosine deprotonates upon oxidation. At neutral pH, the tyrosine to Ru(III) electron-transfer reaction occurred with a rate constant of $5\times10^4\ s^{-1}$ [40], which is slow relative to the oxidation rate of Y_Z in the native enzyme [41]. In manganese-depleted photosystem II samples, however, the oxidation rate of Y_Z is reduced about a thousandfold and occurs on the sub-microsecond to microsecond time scale. Sjödin et al. [42] studied the rate of radical formation in the ruthenium/tyrosine complex shown in Fig. 1 as a function of pH

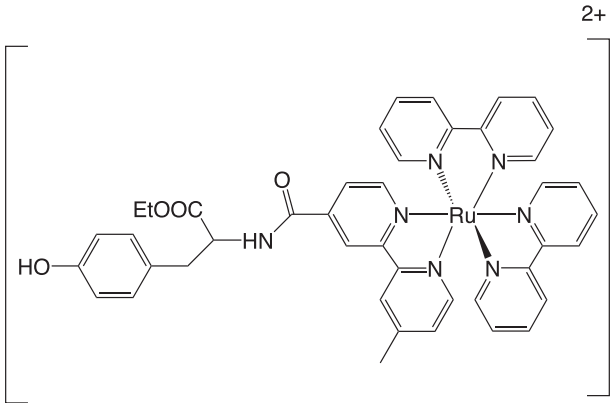

Fig. 1. A Ru(II) tris-bipyridyl complex with a covalently attached tyrosine has been synthesized as a biomimetic model system for the P_{680} and Y_Z redox cofactors in photosystem II [40]. The light-driven radical formation in the model complex has been characterized in detail and compared to the oxidation of Y_Z in manganese-depleted photosystem II [42,43].

and temperature. At pH values below the pK_a of the tyrosine (~10), the rate constant increased from about 3×10^3 s^{-1} at pH 5 to 1×10^5 s^{-1} at pH 9. This pH dependence arises from the fact that although the reduction potential of the Ru(III)/Ru(II) redox couple is pH-independent, the potential of the $Y^{\cdot}/Y$ pair decreases by 59 mV per pH unit at 25° C. Thus, the driving force for the electron-transfer reaction increases as the pH becomes more alkaline. In contrast, at pH values above the pK_a of the tyrosine, the oxidation occurs with a pH-independent rate constant of about 2×10^7 s^{-1}. The hundredfold increase in the oxidation rate of the tyrosinate species relative to the protonated tyrosine is due to a drop in the reorganization energy associated with the electron-transfer reaction [42]. Sjödin et al. concluded that the characteristics observed upon light-excitation of the model complex at pH values below the pK_a of the tyrosine moiety are consistent with a concerted reaction mechanism in which the oxidation and deprotonation of the tyrosine occur simultaneously with a single transition state. A detailed discussion on the proton-coupled electron transfer occurring in the ruthenium/tyrosine model system and comparisons with Y_Z oxidation in manganese-depleted photosystem II can be found in Ref. [43].

Stubbe, Nocera and their respective co-workers have explored several methods for fast amino-acid radical initiation in order to study proton coupled electron-transfer reactions in the class I ribonucleotide reductases [12,44,45]. These enzymes are composed of two homodimeric subunits denoted R1 and R2. The former contains the site of nucleotide reduction while the radical-generating tyrosine/di-iron center is located on the R2 subunit. High-resolution structures have been obtained for the R1 and/or R2 subunits from different organisms, although structural information for the fully active R1/R2 complex is still lacking. Docking studies using the R1 and R2 crystal structures of the *E. coli* enzyme revealed that the active site and the tyrosyl radical/binuclear metal site are spaced widely apart. In the *E. coli* R1/R2 structural model, the distance between the redox-active Tyr-122 and the active-site Cys-439 is estimated to about 35 Å [9,11]. Thus, catalysis involves long-range radical transfer between Tyr-122 and Cys-439. Structural and site-directed mutagenesis studies have identified a possible pathway for this process [9,11]. The proposed 35-Å electron/proton transfer pathway is initiated at Tyr-122 and propagated via Trp-48 and Tyr-356 on the R2 subunit. It crosses the R1/R2 interface, continues with the R1 Tyr-731 and Tyr-730 residues and ends at Cys-439.

The characteristics of caged aromatic amino acids have been investigated with the aim to develop light-dependent methods to oxidize Cys-439 and trigger the catalytic cycle in the absence of the R2 subunit [44,45]. This approach is based on the fact that short peptides from the C-terminus of R2 associate with R1. Thus, a photoactive residue can be incorporated into a chemically synthesized peptide, which in turn, binds to the R1 subunit. An initial study from the Stubbe laboratory showed that a neutral tryptophanyl radical could be generated by laser flash photolysis of an *N*-hydroxypyridine-2-thione tryptophan derivative [44]. The photolysis reaction of this compound using excitation light of 355 nm was remarkably efficient with a quantum yield of 1.0±0.1. In a more recent report, it was shown that photolysis of oxalate-modified tyrosine derivatives can generate tyrosyl radicals on the nanosecond time scale (Fig. 2; Ref. [45]). Various approaches to trigger rapid radical initiation in the ribonucleotide reductase system are described in Ref. [12].

2.2. Rhenium-modified proteins

In addition to using ruthenium to trigger electron-transfer reactions, the Gray laboratory has extended their work on metal-modified redox proteins to include a rhenium-based photosensitizer [46,47]. Cyclic voltammetry on [rhenium(I)(tricarbonyl)(1,10-phenantroline)(imidazole)]$^+$ showed that the Re(II)/Re(I) redox pair has a reduction potential of 1.85 V vs. SCE in acetonitrile [46]. Electrochemical characterization of tyrosine and tryptophan in aqueous buffer display pH-dependent peak potentials, which at pH 7.0 and relative to the NHE has a value of 0.83 V for the former amino acid and 0.89 V for the latter [32]. Thus, the Re(II) state is a powerful oxidant that should be able to generate tyrosyl and tryptophanyl radicals at a fairly high driving force. Di Bilio et al. [47] showed that aromatic amino-acid radicals indeed can be generated in rhenium-modified proteins. Fig. 3 shows the structure of the blue copper protein azurin with a rhenium complex attached to the protein surface. Highlighted in the figure are the copper site and the rhenium complex, which is attached to histidine 107. Also shown in the figure is tyrosine 108. This residue could be selectively oxidized and the radical state trapped at low temperatures by preparing a rhenium-containing azurin sample in which the copper was substituted with zinc and a

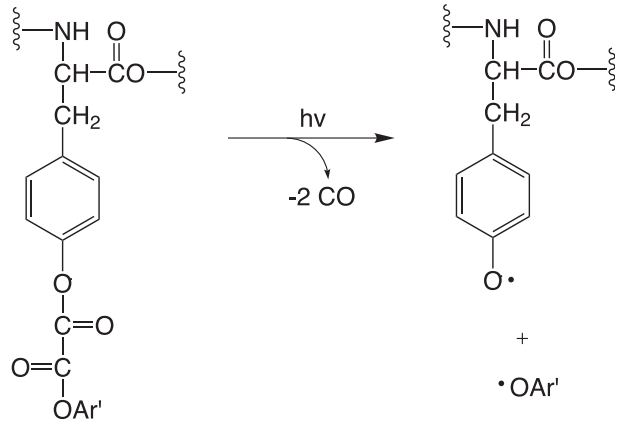

Fig. 2. An example of a caged amino acid used to rapidly form a tyrosyl radical in a light-dependent reaction [45]. The C–O bond is cleaved by laser flash photolysis producing two equivalents of carbon monoxide, an aryloxyl radical and a tyrosyl radical. The aryloxyl radical is sterically protected, which makes the tyrosyl radical the only reactive species on the sub-microsecond time scale.

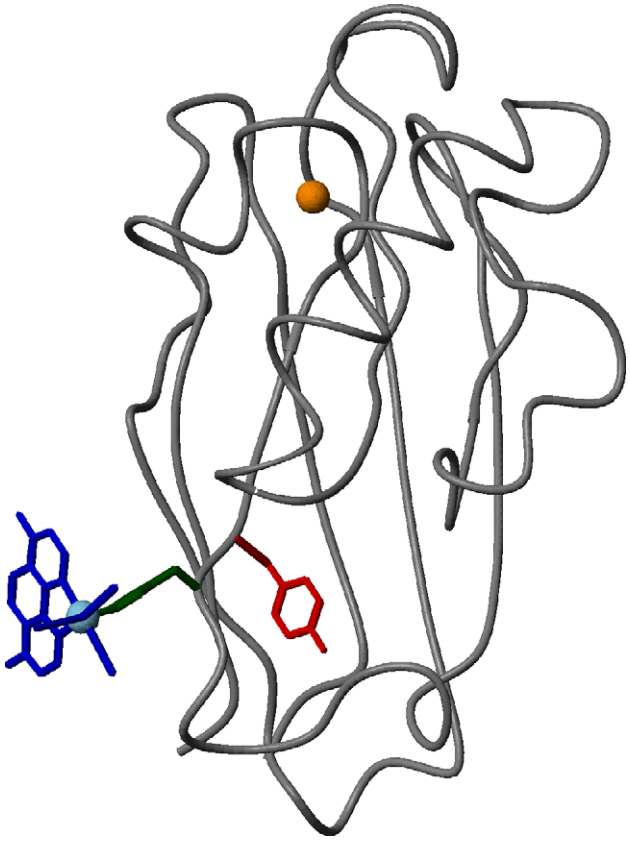

Fig. 3. The structure of a rhenium-modified azurin protein that is capable of tryptophanyl and tyrosyl radical formation [47] (PDB code 1I53). Highlighted in the structure is the copper site and histidine 107 to which the rhenium complex is attached. Also shown in the figure is the tyrosyl radical site at position 108. Figs. 3–7 were prepared using MOLMOL [81].

sacrificial oxidant was added to the medium. The irradiated freeze-trapped sample gave rise to an EPR spectrum with a line shape characteristic of that of a neutral tyrosyl radical [47]. The radical site could be assigned to position 108, since azurin contains only two tyrosines and the second residue had been mutated to a phenylalanine. A similar set of experiments was done in which the rhenium complex was tethered to histidine 83, which is close to the single tryptophan in azurin at position 48. The light-irradiated, zinc-substituted rhenium-H83 protein gave rise to a low-temperature EPR spectrum that can be assigned to a neutral trytophanyl radical [47]. Interestingly, Di Bilio et al. noted that radical migration to Y108 following W48 formation was not observed in the rhenium-H83 protein, as might be predicted from comparing the solution potentials of the two aromatic residues (see above). A reason for this observation may be found in the hydrogen-bonding environment of Y108. In the rhenium-H83 protein, the tyrosine is involved in a bifurcated hydrogen bond to a backbone nitrogen and a carboxyl oxygen of a glutamate residue. In the rhenium-H107 system, the hydrogen bond to the glutamate is broken and the tyrosine hydroxyl group becomes more exposed to the bulk medium. The authors concluded that the increase in solvent exposure facilitates the deprotonation and oxidation of the tyrosyl side chain in the rhenium-H107 protein. In a recent report on the modified azurin system, the spectroscopic and chemical properties of an unusually long-lived tryptophan radical are described [48].

2.3. Redesign of a photosynthetic reaction center

The reduction potential of the P_{680}^{+} /P_{680} redox couple in photosystem II has been estimated to be ~1.2 V vs. NHE [33]. The potentials of the photochemically active bacteriochlorophyll dimers ($BChl_2$) found in the reaction centers of photosynthetic bacteria are substantially less oxidizing [49]. The high reduction potential that drives the water-splitting chemistry in photosystem II is not required for the light-driven electron transport catalyzed by these species since water is not used as the electron source. How the protein environment tunes the properties of the reaction-center pigments in different photosynthetic organisms has for a long time been an area of intense research activity [49,50].

Lin et al. [51] performed a careful investigation on how the reduction potential of the $BChl_2$ species in the reaction center of the purple bacterium *Rhodobacter sphaeroides* is influenced by hydrogen-bonding interactions to surrounding side chains. In the wild type, a hydrogen bond is present between a histidine and one of the acetyl groups involved in the conjugated π-system of the bacteriochlorophyll dimer. Upon removal of this interaction by mutating the histidine to a phenylalanine, the $BChl_2$ potential drops from 505 to 410 mV. The addition of a hydrogen bond to a carbonyl group of the dimer raises its potential and, interestingly, the effects of the single-point mutations are additive. By using various single, double and triple mutants, the $BChl_2$ potential could be tuned within the range of 410–765 mV [51]. Subsequently, this observation was used to engineer a mutant in which the $BChl_2$ reduction potential was elevated to above 800 mV [52]. This was achieved by creating a quadruple mutant in which the number of hydrogen bonds to the conjugated carbonyl groups of the dimer was maximized. Fig. 4 shows the two macrocycles of the *Rb. sphaeroides* bacteriochlorophyll dimer and the four amino-acid residues that were mutated to make this dramatic change in the thermodynamic properties of the reaction center. In addition to mutating the four residues shown in Fig. 4, Kálmán et al. [52] introduced a tyrosine at positions analogous to the Y_Z or Y_D site in photosystem II. The resulting constructs were designated as the Y_M and Y_L mutant, respectively. Following light excitation, the optical and EPR spectra of these two strains changed in a manner consistent with tyrosine oxidation. The spectra represent a mixture of $BChl_2$ and tyrosyl radicals whose relative contributions were sensitive to the bulk pH with alkaline conditions favoring the latter. The yield of the tyrosyl radical formed in the Y_M strain titrates with a pK_a of 6.9 [52]. The structural origin of this pK_a was

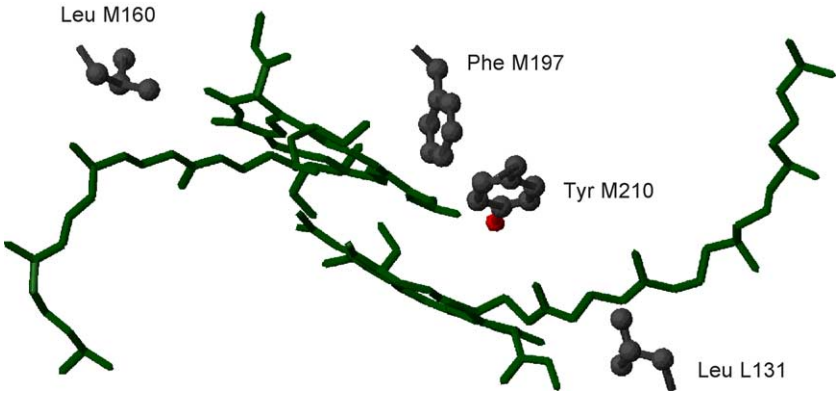

Fig. 4. The photochemically active bacteriochlorophyll dimer in the reaction center of the purple bacterium *Rb. sphaeroides* (PDB code 4RCR). The macrocycles of the pigments are oriented perpendicular to the plane of the paper. Shown in the figure are the four amino acids (leucine 131 in the L subunit; leucine 160, phenylalanine 197 and tyrosine 210 in the M subunit) that were targeted by site-directed mutagenesis to raise the reduction potential of the bacteriochlorophyll dimer above 800 mV [52].

investigated in a recent study [53], which provided data that are in nice agreement with results obtained from photosystem II studies.

In photosystem II, the rate of Y_Z oxidation and the radical yield are strongly influenced by a histidine located at position 190 on the D1 reaction-center protein. About 15 D1-H190 mutants have been constructed and characterized (see Ref. [54] and references therein). At neutral pH, the Y_Z oxidation rate is more than three orders of magnitude slower in these mutants relative to the wild-type system at similar conditions. The oxidation efficiency of Y_Z can be partially recovered in the D1-H190 mutants by raising the pH or, more interestingly, by the addition of an exogenous base that is small enough to access the tyrosine site and functionally substitute for the histidine. In the wild type, the Y_Z oxidation efficiency titrates with a pK_a around 7.0. In the D1-H190 to alanine mutant, the rate of Y_Z oxidation titrates with an apparent pK_a of 10.3, which has been assigned to the tyrosine itself. Notably, upon the addition of a small proton acceptor to the sample buffer, this apparent pK_a value shifts and becomes the same as the solution pK_a of the exogenous base. On the basis of these results, it has been proposed that histidine 190 is involved in a hydrogen-bonded network that accepts the phenol proton when Y_Z is oxidized (for a more detailed discussion, see Refs. [41,54]). Glutamate 189 on the D1 protein has been also been proposed to be involved in this network [54].

Similarly, structural modeling of the *Rb. sphaeroides* Y_M mutant predicts that the introduced tyrosine forms a hydrogen bond to a histidine residue and that it also interacts weakly with a nearby glutamate [53]. Substitution of this histidine to a tyrosine or glutamate increases the pK_a from 6.9 to 8.9. A histidine to glutamine substitution increases the pK_a even further, indicating direct titration of the tyrosine. When both the histidine and the glutamate predicted to interact with the tyrosine are changed into glutamine residues, radical formation is abolished. The authors concluded that the histidine and the glutamate residues serve as proton acceptors for the oxidized tyrosine [53]. These results support the proposal that a proton acceptor is essential in order to lower the reduction potential of a buried tyrosine into a range accessible by natural oxidants [33]. Exactly how the hydrogen-bonding geometry, the existence of one or several connected proton acceptors and their respective pK_a values affect the thermodynamic and kinetic redox properties of functionally essential tyrosines remain to be characterized in more detail.

3. Construction of amino-acid radical maquettes

An additional approach to gain insights into the properties of amino-acid radicals is to synthesize de novo designed model proteins, molecular maquettes [55], in which the redox chemistry of these species can be studied. Natural amino-acid radical enzymes are often highly complex structures containing multiple protein subunits and cofactors. The aim with the construction of de novo radical maquettes is to introduce the radical properties of interest as well as to build in features that will facilitate the biophysical characterization of the system. As described in more detail below, simplicity dominates the first generation of de novo designed radical proteins. The complexity of the system will be increased in a stepwise manner once the initial designs have been characterized. By this approach, we hope to be able to address issues that have been difficult to study in the natural systems. For example, the reduction potentials of buried amino-acid redox cofactors, and how these values change as a function of the protein environment, are to a large extent unknown today. Below we provide a brief background to de novo protein design strategies and then describe the synthesis and characterization of model proteins that have been designed to study amino-acid redox chemistry.

3.1. De novo protein design

The construction of proteins from scratch, de novo design, provides a novel approach to explore protein structure/function relationships that complement and extend more traditional studies on biological systems [56]. Over the past two decades, de novo protein design has progressed from the design of simple secondary structures such as monomeric α-helices [57] to synthesizing proteins with catalytic activity [58–60]. Iterative rational design, template-assembled strategies, and computational and combinatorial methods have been used to create structures containing interacting α-helices [56,59–62], β-sheets [59,63,64] and mixed α/β folds [65,66].

Early efforts in de novo protein design were mainly focused on delineating the parameters involved in the formation and stabilization of α-helical structures. The individual α-helical propensities of the amino acids, hydrogen-bonding interactions capping the C- and N-termini, and side-chain/side-chain and side-chain/helix dipole electrostatic interactions have been shown to be important for the stabilization of monomeric α-helices in aqueous solution [57]. A structural investigation of the two stranded coiled-coil protein tropomyosin provided insights into the factors that drive the association of α-helices into oligomeric structures. Hodges et al. [67,68] found a repeating seven-residue (heptad) pattern of hydrophobic and hydrophilic amino acids spanning the tropomyosin sequence. A heptad repeat, denoted $(abcdefg)_n$ [69], typically contains hydrophobic residues at positions *a* and *d*, charged residues at *e* and *g*, and polar side chains at *b*, *c* and *f*. Upon oligomerization, the residues at the *a* and *d* positions form the hydrophobic core of the protein while the charged residues at the *e* and *g* positions make the boundary of the core and provide stabilizing electrostatic interactions between the associating α-helices. The residues in remaining positions create the hydrophilic surface of the protein. In a subsequent study from the Hodges group, it was demonstrated that a heptad repeat pattern could be used to create de novo designed two-stranded coiled coils [70].

Following these initial studies, design principles for synthesizing more complex coiled coils and α-helical bundle proteins emerged. The design of the heptad repeat and particularly the choice of the hydrophobic and the charged residues proved to be essential for determining the oligomerization state and the conformational specificity of the designed protein. Early de novo designs typically contained only leucine residues in the heptad *a* and *d* positions, which gave rise to dynamic and structurally ill-defined hydrophobic cores. Aromatic and β-branched amino acids have few allowed rotamers on the α-helix and the introduction of these types of residues at the heptad *a* and *d* positions reduces the dynamic disorder and contributes to structural specificity [71–73]. The hydrophobic core residues must also be complementary in shape. A combination of small and large side chains at each core layer is important to provide a well-packed protein interior [71,74]. In addition, negative design strategies can be used in order to obtain conformational specificity and avoid an ensemble of non-native and partially folded states [75]. The key concept with negative design is to energetically favor one structure by giving alternative structures energy penalties, as for example by introducing unfavorable electrostatic interactions. Based on the design concepts described above, three-helix bundle and four-helix bundle proteins have been synthesized and structurally characterized by NMR spectroscopy [21,76–78]. Since a high-resolution NMR structural model only can be obtained for a uniquely structured protein, these detailed spectroscopic studies are important both in order to evaluate the designs and to demonstrate that conformational specificity has been obtained.

Recently, progress has also been made in designing more complex folds. NMR structural models of de novo designed β-sheets and proteins containing mixed α/β secondary structures have been achieved using iterative rational design and computational methods [63–66]. One pronounced obstacle in the design of β-sheets is that these constructs have a tendency to aggregate [59,79]. Moffet and Hecht [59] have used binary code strategies to construct combinatorial libraries of de novo designed four-helix bundles and of β-sheet proteins. Structural characterization of the proteins generated from the β-sheet libraries showed that indeed β-sheets were formed but that they aggregate into amyloid-like fibrils. The Hecht group subsequently used rational design to address this issue. Hydrophobic residues at solvent exposed sites were mutated to lysines and these mutations resulted in a conversion of the fibril structures into monomeric β-sheet proteins [80].

In particular, the α-helical bundle scaffold has been explored to design holoproteins containing a range of different metals and cofactors including hemes, iron-sulfur clusters, copper ions and flavins [56,61]. These studies have illustrated the utility of using designed proteins to, e.g., characterize electron transfer between relatively low potential cofactors. The research described below is aimed to apply the de novo design strategy to the investigation of the high potential redox cofactors found in amino-acid radical enzymes.

3.2. De novo radical protein design

Tryptophan and tyrosine are found as the catalytic species in the majority of amino-acid radical enzymes and, accordingly, our main emphasis is on these residues. Fig. 5 shows structural models of two α-helical proteins, denoted α_3W and α_4W, that have been constructed with the aim of investigating tryptophan and tyrosine redox chemistry. α_3W and α_4W were designed to contain the following key features: (i) The protein should be a monomeric three-helix (α_3W) or four-helix (α_4W) bundle containing a single tryptophan or tyrosine. (ii) The aromatic residue should be buried, rather than

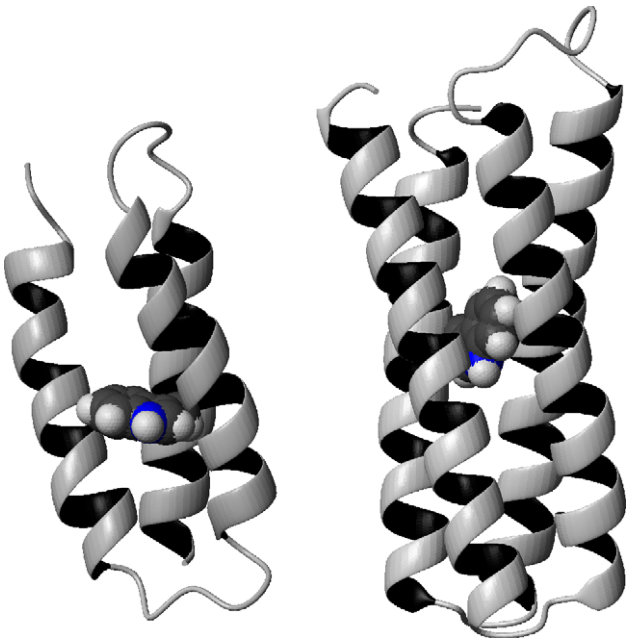

Fig. 5. Two α-helical protein scaffolds, a three-helix bundle (α_3W) and a four-helix bundle (α_4W), that have been designed and synthesized with the aim to study tryptophan and tyrosine radical chemistry in a protein milieu. The structure of the de novo designed α_3W protein has been experimentally determined by NMR spectroscopy [21]. The α_4W structure is a design model based on the coordinates of the DNA-binding protein Rop [85].

located in a solvent-exposed position in which solution conditions are expected to dominate its chemistry. (iii) The remaining residues should be redox inert in order to isolate the radical chemistry to a single site. α_3W has been synthesized both chemically and biochemically and the protein samples have been characterized by a range of biophysical methods. The results of these studies are described below. The construction of the α_4W protein is more recent and we will present some preliminary results on this system.

3.3. Initial characterization of α_3W and α_3Y

The 65-residue peptide chain of α_3W is based on the heptad repeat design strategy discussed in Section 3.1. The α_3W sequence is shown below with each heptad segment separated by bullets and the *a* and *d* positions marked in bold.

R · **V**KA**L**EEK · **V**KA**L**EEK · **V**KA**L** – *GGGG* – R

· **I**EE**L**KKK · **W**EE**L**KKK · **I**EE**L** – *GGGG* – E

· **V**KK**V**EEE · **V**KK**L**EEE · **I**KK**L**

The sequence is designed to contain three interacting α-helices each containing 19 amino acids. The three helical regions are linked by two glycine loops containing four residues each. The unique tryptophan is placed on the second helix in position 32. Residue 32 is at a heptad *a* position and is thus predicted to be located in the hydrophobic core of the protein.

α_3W and its tyrosine derivative α_3Y were initially synthesized by solid-phase peptide synthesis [32]. The protein sequence of α_3Y is identical to the sequence of α_3W with the exception of residue 32, which in α_3Y is changed to a tyrosine. Following chemical synthesis and HPLC purification, the α_3W and α_3Y samples were characterized in order to investigate the degree of α-helical content, the thermodynamic stability, the conformational specificity and the aggregation state of the two proteins. Using CD spectroscopy, the α-helical content of α_3W and α_3Y was estimated to about 70% over a pH range of 4 to 10. The thermodynamic stability of the two proteins was determined by chemical denaturation and amide ^{1}H/^{2}H isotope-exchange measurements. These studies showed that the stability of the designed three-helix bundles was within the range reported for natural proteins of similar size. With de novo protein design, a major challenge is to obtain conformational specificity, i.e., to create a protein sequence that folds into a unique structure in solution. The construction of a de novo protein is an iterative process in which NMR spectroscopy often is used to evaluate the properties of the intermediate designs. An NMR spectrum exhibiting a single set of resonances with narrow line widths and a large chemical-shift dispersion is characteristic of a protein with well-defined secondary and tertiary structures. Poor chemical-shift dispersion, and multiple and/or broadened magnetic resonances are, in contrast, indicative of a dynamic ensemble of interchanging conformations. One-dimensional ^{1}H spectra and two-dimensional natural abundance ^{13}C HSQC spectra were obtained on α_3W and α_3Y. Both the 1D and 2D NMR data displayed spectral characteristics that are consistent with uniquely structured proteins. In addition to the spectroscopic studies, size-exclusion chromatography and analytical sedimentation equilibrium ultracentrifugation were performed to determine the aggregation state of the proteins. These measurements confirmed that the three-helix bundles are monomeric in solution. Finally, the local environments of the aromatic residues were studied in more detail. The fluorescence spectrum of Trp-32 in α_3W has an emission maximum that is blue-shifted by 28 nm relative to the spectrum of tryptophan free in solution. The pK_a of Tyr-32 in α_3Y is up-shifted by more than 1.2 pH units as compared to tyrosine dissolved in water. These characteristics suggest that the two aromatic residues are sequestered from the bulk medium. This conclusion was further strengthened by NOESY data, which revealed a number of short-range magnetic interactions between the protons associated with the aromatic head groups of Trp-32 and Tyr-32 and methyl and other aliphatic protons. The NOESY spectra indicate that the aromatic rings are located in the protein interior since aliphatic residues form the hydrophobic cores of the three-helix bundles.

In addition to a structural characterization, the redox properties of the two de novo designed radical proteins were probed by differential pulse voltammetry [32]. The electro-

chemical studies revealed that the peak potentials of Trp-32 and Tyr-32 are significantly elevated relative to the potentials measured for tryptophan and tyrosine dissolved in aqueous buffer. For example, at pH 10 the potential of Trp-32 was 0.35 V more oxidizing than tryptophan free in solution.

Thus, the initial structural characterization of α_3W and α_3Y provided data that are consistent with two stable, uniquely structured α-helical proteins, each containing a single aromatic side chain residing in a hydrophobic environment [32]. This conclusion was confirmed in a subsequent study in which the NMR solution structure of α_3W was obtained [21]. In addition, the NMR work revealed a cation-π interaction between Trp-32 and a nearby lysine residue. The effects of this interaction on the reduction potential of the tryptophan side chain were investigated using density-functional theory and the theoretical study provided data that are consistent with the electrochemical characterization of α_3W. The structural and quantum chemical analyses of α_3W are described in the sections that follow.

3.4. Structural characterization of α_3W

The initial characterization of α_3W was performed on protein samples that were produced by chemical synthesis. For a detailed structural analysis of α_3W, however, ^{13}C and ^{15}N enriched protein material was required. A bacterial expression system was developed to induce the synthesis of the three-helix bundle in *E. coli* cells cultivated on isotopically enriched medium [21]. The three-helix bundle was co-expressed as a fusion with thioredoxin. A glycine-serine addition remains in the N-terminus of α_3W following thrombin digestion of the fusion protein to remove thioredoxin. In order to keep the amino-acid numbering consistent between the chemically synthesized (65 residues) and the bacterially expressed proteins (67 residues), we number the GS extension as −2 and −1, respectively.

As shown in Fig. 6A, a high-quality structural model of GS-α_3W could be obtained by using multi-dimensional NMR techniques [21]. The experimentally determined structure confirms the design of the radical maquette and shows that the peptide chain of GS-α_3W folds into a compact three-helix bundle in solution. The core of the protein is composed of six hydrophobic layers with Trp-32 located in one of the two central layers (Fig. 6B). A key design feature of the de novo radical protein was that the aromatic residue should be sequestered from the bulk solution (see Section 3.2). The MOLMOL [81] program was used to calculate the accessible surface area of Trp-32. The analysis showed that 2.6% of the Trp-32 surface area is accessible to the bulk solvent. This value represents an average of the accessibility value calculated for each of the 16 structures in the NMR family. The range in the accessible surface area for the whole structural family was 0.8–6.1%. The observed accessibility is essentially exclusively associated with the indole group having a 5.5 (0–41.9)% accessibility of the nitrogen atom and a 28.8 (8.5–63.1)% exposure of its bound hydrogen atom. Thus, we conclude that the experimentally derived structure of GS-α_3W fulfills the design criteria defined for the first generation of de novo radical proteins.

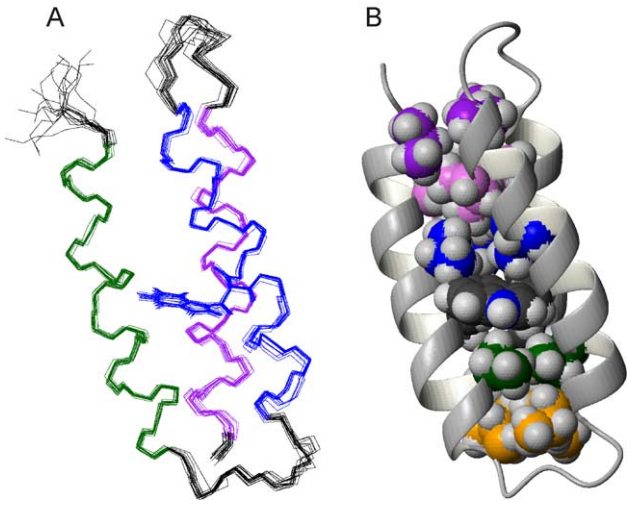

Fig. 6. (A) Solution structure of the de novo designed radical maquette GS-α_3W [21] (PDB code 1LQ7). The structure is displayed as a backbone superposition of the refined family of GS-α_3W structures. Helical regions are shown in green (residues 2–18), blue (residue 25–41) and purple (residue 48–64). Shown in blue are the heavy amino-acid atoms of the unique tryptophan at position 32. The average pairwise rmsd values for the structural model are: 0.76±0.18 Å for the backbone atoms of all residues, 0.32±0.10 Å for the backbone atoms of the residues in the helical regions, 1.29±0.11 Å for the heavy atoms of all residues, and 1.11±0.13 Å for the heavy atoms of the residues in the helical regions. (B) Packing of the interior side chains of GS-α_3W. The main part of the protein hydrophobic core consists of six layers of heptad *a* and *d* residues. Each core layer is composed of one side chain derived from each of the three individual helices. The composition of the core layers is as follows: V2, L42, V48 (purple); L5, I39, V51 (violet); V9, L35, V55 (blue); L12, W32, L58 (grey/blue); V16, L28, I62 (green); L19, I25, L65 (yellow). Although not shown in the figure, residues in heptad *e* and *g* positions also contribute to the hydrophobic volume of GS-α_3W.

The NMR structural study also revealed that Trp-32 is involved in a cation-π interaction with Lys-36, which is located one helical turn away from the aromatic residue. The structural arrangement of the Trp-32/Lys-36 pair is shown in Fig. 7. Recent studies of the Protein Data Bank have shown that cation-π interactions between aromatic (Phe, Trp, Tyr) and cationic (Arg, Lys) side chains are common in natural proteins [82–84]. For example, Gallivan and Dougherty [83] analyzed 593 protein structures using energy-based criteria and concluded that 26% of the tryptophan residues are involved in an energetically significant cation-π interaction. The apparent high frequency of this structural motif suggests that it could have a significant influence over the thermodynamic properties of tryptophans in proteins. The electrochemical characterization of α_3W suggests that a cation-π interaction will increase the reduction potential of tryptophan [21,32]. A theoretical analysis confirms this conclusion, as described below.

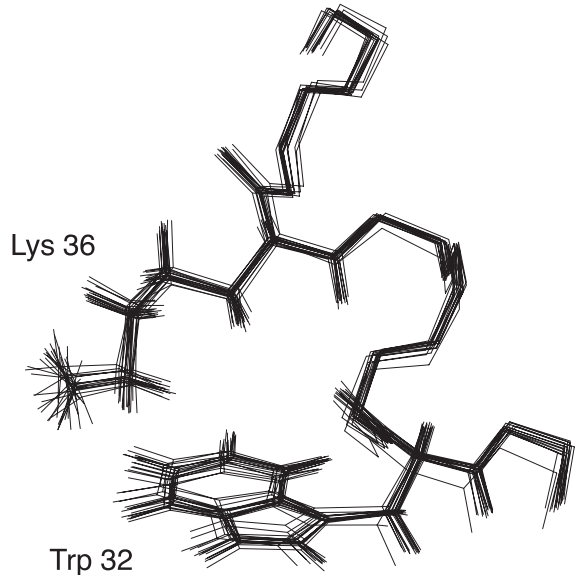

Fig. 7. As illustrated in the figure, the de novo designed GS-α_3W protein contains a cation-π interaction between Trp-32 and Lys-36 [21]. Since this type of interaction is common in natural proteins [82–84], it was interesting to investigate the thermodynamic properties of a tryptophan engaged in a cation-π interaction. Experimental and theoretical studies of the radical maquette showed that the tryptophan reduction potential increases in the presence of the cation-π interaction (see text for a detailed discussion).

3.5. The influence of a cation-π interaction on the thermodynamic properties of tryptophan

For the oxidation of a tryptophan, we have three possible events to consider: (1) the oxidation of the reduced and protonated (WH) species to a tryptophanyl cation radical ($W^{\cdot}H^{+}$), $WH \rightarrow W^{\cdot}H^{+}+e^{-}$; (2) the oxidation of the reduced and protonated tryptophan to a neutral radical ($W^{\cdot}$), $WH \rightarrow W^{\cdot}+H^{+}+e^{-}$; (3) the oxidation of the deprotonated tryptophanyl anion (W^{-}) to a neutral radical, $W^{-} \rightarrow W^{\cdot}+e^{-}$. Reaction 3 can be excluded due to the high pK_a of the reduced form of Trp-32. The optical spectrum of Trp-32 remains invariant from pH 4 to 13.5, which means that deprotonation of the indole head group does not occur within this pH range [32]. Thus, the two redox couples that are relevant to consider are $W^{\cdot}H^{+}$/WH and $W^{\cdot}$/WH (reactions 1 and 2). That the reduction potential of the $W^{\cdot}H^{+}$/WH redox pair will increase in the presence of a cation-π interaction is clear from electrostatic reasons. The formation of a cation radical in close proximity to a protonated lysine is an energetically unfavorable state. Thus, a cation-π interaction will stabilize the reduced state and it will destabilize the oxidized state. These effects will give rise to an overall increase in the reduction potential of the $W^{\cdot}H^{+}$/WH redox couple. The magnitude of the increase will be determined by the strength of the cation-π association and the local dielectric constant of the protein medium.

The effect of the cation-π interaction on the reduction potential of the $W^{\cdot}$/WH redox pair is more difficult to predict. If the cation-π interaction is stronger to the reduced tryptophan relative to the neutral radical state, the reduction potential is expected to increase. In contrast, the potential will decrease if the cation-π interaction stabilizes the oxidized tryptophan more than the reduced species. We addressed this issue by calculating the effects of the cation-π interaction on the indole N–H bond dissociating energy using hybrid density functional theory [21]. The N–H bond strength was calculated in the absence and presence of cation-π interaction in the gas phase and in a dielectric medium of 4 and 80. In the presence of a cation-π interaction, the N–H bond dissociating energy increased by 6.8 kcal mol^{-1} in the gas phase. The increase was 3.2 kcal mol^{-1} at a typical protein dielectric constant of 4. Finally, at a dielectric constant of 80 the increase was 1.4 kcal mol^{-1}. Since it is the N–H bond that breaks upon the oxidation of a tryptophan to a neutral radical, these results predict that the reduction potential of the $W^{\cdot}$/WH redox pair will increase if the indole ring is involved in a charge-π interaction. The observed increase in the bond-dissociation energy for the tryptophan N–H group in the presence of the lysine can be understood as follows. The cation-π association is an interaction between the π electrons associated with the aromatic ring of the tryptophan and the charge on the protonated lysine residue. In its oxidized form, the tryptophan contains one less electron relative to its reduced form and, consequently, the charge-π interaction becomes weaker. Thus, the cation-π interaction stabilizes the reduced form of the tryptophan relative to its oxidized form and, consequently, it becomes more difficult to oxidize the aromatic residue.

Our first set of calculations was done using an indole/methylammonium model system [21]. More recently, we have calculated the N–H bond strength of Trp-32±a cation-π interaction to Lys-36 by using the coordinates from the GS-α_3W structure. Preliminary results indicate that the bond dissociation energies derived from the Trp-32/Lys-32 pair are in close agreement with the values given above for the smaller model system (Lundberg, Blomberg, Tommos, unpublished data).

3.6. The design and synthesis of α_4W

With α_3W, we have shown that de novo protein design combined with structural, electrochemical and theoretical analyses can provide detailed information on how the thermodynamic properties of tryptophan are influenced by its protein environment. The larger α_4W protein has been constructed to compliment the work on the three-helix-bundles and expand the family of model radical proteins. The molecular mass of α_4W is 13.0 kDa, which is almost twice the size of the 7.5-kDa α_3W protein. With α_4W, we wish to make similar measurements as with α_3W and study the effects of using a larger protein scaffold, including increased solvent screening, lower dielectric, and so forth, on the radical chemistry.

The sequence of α_4W is derived from an extensive redesign of the RNA-binding protein Rop [85]. Rop is a four-helix bundle consisting of two identical helix-turn-helix subunits arranged in an antiparallel manner. The 63-amino-acid sequence of each Rop monomer is shown below. The residues assigned to the heptad *a* and *d* positions are displayed in bold and the three residues forming the hairpin bend that joins the two α-helices of each subunit is shown in italic [85].

MTKQ · **E**KT**A**LNM · **A**RF**I**RSQ · **T**LT**L**LEK · **L**NE

– ***L****DA* – DE**Q**ADI · **C**ES**L**HDH · **A**DE**L**YRS

· **C**LAR**F**GDDGENL

In α_4W, the two helix-turn-helix subunits are arranged in a parallel topology and linked together by a loop to make the protein monomeric. To introduce this dramatic change in the Rop structure, the hydrophobic core was completely redesigned. In addition, multiple alterations were made at exterior positions including both interhelical and fully solvent-exposed sites. The resulting 117-residue peptide chain of α_4W is shown below with the *a* and *d* positions of the heptad repeats highlighted.

GSKQ · **E**KT**A**LNM · **A**DE**V**RSQ · **T**KT**V**LEK · **L**NK

– ***L****DA* – DE**Q**ADI · **F**KS**L**ADA · **A**DE**L**ERS · **V**KA**R**F

– *GGGGG* – **E**TKQ · **E**KT**A**LNK · **A**RE**I**RSQ

· **T**KT**L**LEK · VNE – ***L****DA* – DE**I**ARV · **A**ES**L**ADA

· **W**DE**L**ERS · **I**KA**R**F

The sequence contains four helical regions, which are designed to contain 26 or 28 amino acids each. The first and the last of the turns between the four helices are conserved from the original Rop sequence, consisting only of a leucine and an aspartic acid. The central loop is longer and contains five glycine residues. The protein core is design to contain eight hydrophobic layers. The unique tryptophan is placed at position 106, a heptad *a* site in layer five of the hydrophobic core.

As described above, the 65-residue three-helix bundles were first synthesized by solid-phase peptide synthesis and then recombinantly expressed in *E. coli*. A major advantage with chemical synthesis is that protein samples can be generated fairly quickly, typically on the week time scale. To synthesize a gene and construct a bacterial expression system usually takes months rather than weeks. Once an efficient expression system has been obtained, however, making mutants and producing high quantities of both regular and isotopically enriched protein samples can be done quickly. With the monomeric three-helix bundle, we had the advantage that we could do an initial characterization on chemically generated samples to probe the design and then do more detailed studies on biochemically produced samples. The construction of a monomeric four-helix bundle protein is more challenging since chemical synthesis of the 117-amino-acid sequence is not expected to generate sufficient material for the initial biophysical characterization of the protein. Thus, with α_4W, we had to go directly from designing the peptide sequence to the construction of an expression system.

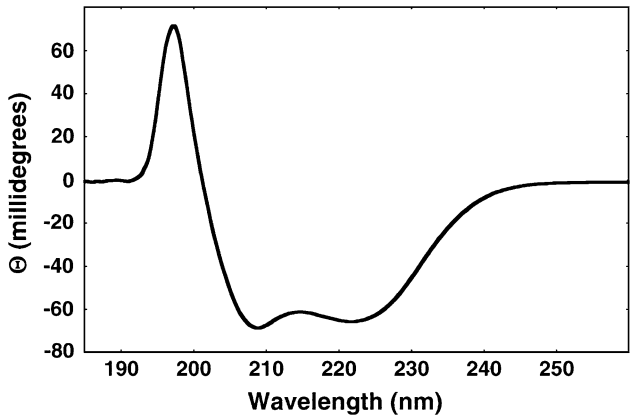

Fig. 8. CD spectrum of α_4W (18 μM protein, 10 mM K_2HPO_4 pH 7.0, 15 mM KCl) obtained at 25 °C.

The α_4W gene was designed by back-translating the protein sequence using *E. coli* preferred codons. Start and stop codons and *Bam*H1 and *Eco*R1 restriction enzyme sites were added to the flanking regions of the resulting DNA fragment. A nested PCR strategy was used to assemble the complete 388 base pair sequence [86]. Following sequence verification, the α_4W gene was ligated into a modified [77] Novagen pET protein expression vector and transformed into *E. coli*. α_4W is expressed as a thioredoxin fusion protein in the same manner as α_3W. Following thrombin digestion and HPLC purification, the molecular mass of α_4W was verified by mass spectrometry (calculated mass, 12 980.1 Da; experimental mass, 12 980.5 Da).

An initial CD characterization of α_4W shows the structure to be about 60% helical (Fig. 8). A guanidine hydrochloride chemical melt of α_4W provided a free energy of unfolding of −4.0 kcal mol^{-1} and an *m* value of 4.8 kcal mol^{-1} M^{-1} (data not shown). Addition studies, similar to those described in Section 3.3, are in progress to evaluate the properties of α_4W. We note that the sequence shown above represents the first design of the monomeric four-helix bundle and it is likely to evolve as the structural properties of α_4W are refined via an iterative design process.

Acknowledgements

The design of the α_4W protein was done in collaboration with Professor Brian Gibney at Columbia University, New

York. The modified pET32b vector used for the α_4W expression system was a kind gift from Professor A. Joshua Wand at the University of Pennsylvania, Philadelphia. This work was funded by the Swedish Research Council. H.K.P. gratefully acknowledges support from the Swedish-American Fulbright Commission.

References

[1] J. Stubbe, W.A. van der Donk, Protein radicals in enzyme catalysis, Chem. Rev. 98 (1998) 705–762.
[2] F. Himo, P.E.M. Siegbahn, Quantum chemical studies of radical-containing enzymes, Chem. Rev. 103 (2003) 2421–2456.
[3] M.Z. Hoffman, E. Hayon, Pulse radiolysis study of sulfhydryl compounds in aqueous solution, J. Phys. Chem. 77 (1973) 990–996.
[4] D.V. Bent, E. Hayon, Excited state chemistry of aromatic amino acids and related peptides: I. Tyrosine, J. Am. Chem. Soc. 97 (1975) 2599–2606.
[5] J.F. Baugher, L.I. Grossweiner, Photolysis mechanism of aqueous tryptophan, J. Phys. Chem. 81 (1977) 1349–1354.
[6] V.-M. Leppänen, M.C. Merckel, D.L. Ollis, K.K. Wong, J.W. Kozarich, A. Goldman, Puruvat formate lyase is structurally homologous to type I ribonucleotide reductase, Structure 7 (1999) 733–744.
[7] A. Becker, K. Fritz-Wolf, W. Kabsch, J. Knappe, S. Schultz, A.F.V. Wagner, Structure and mechanism of the glycyl radical enzyme pyruvat formate-lyase, Nat. Struct. Biol. 6 (1999) 969–975.
[8] J.W. Whittaker, Free radical catalysis by galactose oxidase, Chem. Rev. 103 (2003) 2347–2363.
[9] M. Sahlin, B.-M. Sjöberg, Ribonucleotide reductase: a virtual playground for electron transfer reactions, in: A. Holzenburg, N.S. Scrutton (Eds.), Enzyme-Catalyzed Electron and Radical Transfer, Sub-Cellular Biochemistry, vol. 35, Kluwer Academic Publishing/Plenum, New York, 2000, pp. 405–443.
[10] J. Stubbe, J. Ge, C.S. Yee, The evolution of ribonucleotide reduction revisited, Trends Biochem. Sci. 26 (2001) 93–99.
[11] H. Eklund, U. Uhlin, M. Färnegårdh, D.T. Logan, P. Nordlund, Structure and function of the radical enzyme ribonucleotide reductase, Prog. Biophys. Mol. Biol. 77 (2001) 177–268.
[12] J. Stubbe, D.G. Nocera, C.S. Yee, M.C.Y. Chang, Radical initiation in the class I ribonucleotide reductase: long range proton-coupled electron transfer?, Chem. Rev. 103 (2003) 2167–2201.
[13] C. Aubert, M.H. Vos, P. Mathis, A.P.M. Eker, K. Brettel, Intraprotein radical transfer during photoactivation of DNA photolyase, Nature 405 (2000) 586–590.
[14] C. Aubert, P. Mathis, A.P.M. Eker, K. Brettel, Intraprotein electron transfer between tyrosine and tryptophan in DNA photolyase from *Anacystis nidulans*, Proc. Natl. Acad. Sci. U. S. A. 96 (1999) 5423–5427.
[15] A. Sancar, Structure and function of DNA photolyase and cryptochrome blue-light photoreceptors, Chem. Rev. 103 (2003) 2203–2237.
[16] J.E. Erman, L.B. Vitello, Yeast cytochrome *c* peroxidase: mechanistic studies via protein engineering, Biochim. Biophys. Acta 1597 (2002) 193–220.
[17] A.-L. Tsai, R.J. Kulmacz, Tyrosyl radicals in prostaglandin H synthase-1 and -2, Prostaglandins Other Lipid Mediat. 62 (2000) 231–254.
[18] A. Ivancich, H.M. Jouve, J. Gaillard, EPR evidence for a tyrosyl radical intermediate in bovine liver catalase, J. Am. Chem. Soc. 118 (1996) 12852–12853.
[19] C. Su, M. Sahlin, E.H. Oliw, A protein radical and ferryl intermediates are generated by linoleate diol synthase, a ferric hemeprotein with dioxygenase and hydroperoxide isomerase activities, J. Biol. Chem. 273 (1998) 20744–20751.
[20] M.A. Miller, G.W. Han, J. Kraut, A cation binding motif stabilizes the compound I radical of cytochrome *c* peroxidase, Proc. Natl. Acad. Sci. U. S. A. 91 (1994) 11118–11122.
[21] Q.-H. Dai, C. Tommos, E.J. Fuentes, M.R.A. Blomberg, P.L. Dutton, A.J. Wand, Structure of a de novo designed protein model of radical enzymes, J. Am. Chem. Soc. 124 (2002) 10952–10953.
[22] G.T. Babcock, B.A. Barry, R.J. Debus, C.W. Hoganson, M. Atamian, L. McIntosh, I. Sithole, C.F. Yocum, Water oxidation in photosystem II: from radical chemistry to multielectron chemistry, Biochemistry 28 (1989) 9557–9565.
[23] D.A. Proshlyakov, M.A. Pressler, C. DeMaso, J.F. Leykam, D.L. DeWitt, G.T. Babcock, Oxygen activation and reduction in respiration: involvement of redox-active tyrosine 244, Science 290 (2000) 1588–1591.
[24] C. Tommos, G.T. Babcock, Oxygen production in nature: a light-driven metalloradical enzyme process, Acc. Chem. Res. 31 (1998) 18–25.
[25] V.L. Pecoraro, M.J. Baldwin, M.T. Caudle, W.-Y. Hsieh, N.A. Law, A proposal for water oxidation in photosystem II, Pure Appl. Chem. 70 (1998) 925–929.
[26] J.S. Vrettos, J. Limburg, G.W. Brudvig, Mechanism of photosynthetic water oxidation: combining biophysical studies of photosystem II with inorganic model chemistry, Biochim. Biophys. Acta 1503 (2001) 229–245.
[27] M. Haumann, W. Junge, Photosynthetic water oxidation: a simplex-scheme of its partial reactions, Biochim. Biophys. Acta 1411 (1999) 86–91.
[28] R.B. Gennis, Multiple proton-conducting pathways in cytochrome oxidase and a proposed role for the active-site tyrosine, Biochim. Biophys. Acta 1365 (1998) 241–248.
[29] A. Sucheta, I. Szundi, Ó. Einarsdóttir, Intermediates in the reaction of fully reduced cytochrome *c* oxidase with dioxygen, Biochemistry 37 (1998) 17905–17914.
[30] F. MacMillan, A. Kannt, J. Behr, T. Prisner, H. Michel, Direct evidence for a tyrosine radical in the reaction of cytochrome *c* oxidase with hydrogen peroxide, Biochemistry 38 (1999) 9179–9184.
[31] M. Fontecave, E. Mulliez, S. Ollagnier-de-Choudens, Adenosylmethionine as a source of 5′-deoxyadenosyl radicals, Curr. Opin. Chem. Biol. 5 (2001) 506–511.
[32] C. Tommos, J.J. Skalicky, D.L. Pilloud, A.J. Wand, P.L. Dutton, De novo proteins as models of radical enzymes, Biochemistry 38 (1999) 9495–9507.
[33] C. Tommos, G.T. Babcock, Proton and hydrogen currents in photosynthetic water oxidation, Biochim. Biophys. Acta 1458 (2000) 199–219.
[34] R.A. Marcus, N. Sutin, Electron transfers in chemistry and biology, Biochim. Biophys. Acta 811 (1985) 265–322.
[35] H.B. Gray, J.R. Winkler, Electron transfer in proteins, Annu. Rev. Biochem. 65 (1996) 537–561.
[36] J.R. Winkler, Electron tunneling pathways in proteins, Curr. Opin. Chem. Biol. 4 (2000) 192–198.
[37] C.C. Page, C.C. Moser, P.L. Dutton, Mechanism for electron transfer within and between proteins, Curr. Opin. Chem. Biol. 7 (2003) 551–556.
[38] F. Millett, B. Durham, Design of photoactive ruthenium complexes to study interprotein electron transfer, Biochemistry 41 (2002) 11315–11324.
[39] M.J. Bjerrum, D.R. Casimiro, I.-J. Chang, A.J. Di Bilio, H.B. Gray, M.G. Hill, R. Langen, G.A. Mines, L.K. Skov, J.R. Winkler, D.S. Wuttke, Electron-transfer in ruthenium-modified proteins, J. Bioenerg. Biomembranes 27 (1995) 295–302.
[40] A. Magnuson, H. Berglund, P. Korall, L. Hammarström, B. Åkermark, S. Styring, L. Sun, Mimicking electron transfer reactions in photosystem II: synthesis and photochemical characterization of a ruthenium(II) tris(bipyridyl) complex with a covalently linked tyrosine, J. Am. Chem. Soc. 119 (1997) 10720–10725.
[41] C. Tommos, Electron, proton and hydrogen-atom transfers in pho-

tosynthetic water oxidation, Philos. Trans.-R. Soc. 357 (2002) 1383–1394.
[42] M. Sjödin, S. Styring, B. Åkermark, L. Sun, L. Hammarström, Proton-coupled electron transfer from tyrosine in a tyrosine-rutheniumtris-bipyridine complex: comparison with tyrosine$_Z$ oxidation in photosystem II, J. Am. Chem. Soc. 122 (2000) 3932–3936.
[43] M. Sjödin, S. Styring, B. Åkermark, L. Sun, L. Hammarström, The mechanism for proton-coupled electron transfer from tyrosine in a model complex and comparison with Y_Z oxidation in photosystem II, Philos. Trans.-R. Soc. 357 (2002) 1471–1479.
[44] D. Burdi, B.M. Aveline, P.D. Wood, J. Stubbe, R.W. Redmond, Generation of a tryptophan radical in high quantum yield from a novel amino acid analog using near-UV/visible light, J. Am. Chem. Soc. 119 (1997) 6457–6460.
[45] M.C.Y. Chang, S.E. Miller, S.D. Carpenter, J. Stubbe, D.G. Nocera, Nanosecond generation of tyrosyl radicals via laser-initiated decaging of oxalate-modified amino acids, J. Org. Chem. 67 (2002) 6820–6822.
[46] W.B. Connick, A.J. Di Bilio, M.G. Hill, J.R. Winkler, H.B. Gray, Tricarbonyl(1,10-phenanthroline) (imidazole)rhenium(I): a powerful photooxidant for investigation of electron tunneling in proteins, Inorg. Chim. Acta 240 (1995) 169–173.
[47] A.J. Di Bilio, B.R. Crane, W.A. Wehbi, C.N. Kiser, M.M. Abu-Omar, R.M. Carlos, J.H. Richards, J.R. Winkler, H.B. Gray, Properties of photogenerated tryptophan and tyrosyl radicals in structurally characterized proteins containing rhenium (I) tricarbonyl diimines, J. Am. Chem. Soc. 123 (2001) 3181–3182.
[48] J.E. Miller, C. Gradinaru, B.R. Crane, A.J. Di Bilio, W.A. Wehbi, S. Un, J.R. Winkler, H.B. Gray, Spectroscopy and reactivity of a photogenerated tryptophan radical in a structurally defined protein environment, J. Am. Chem. Soc. 125 (2003) 14220–14221.
[49] W. Hillier, G.T. Babcock, Photosynthetic reaction centers, Plant Physiol. 125 (2001) 33–37.
[50] P. Heathcote, P.K. Fyfe, M.R. Jones, Reaction centres: the structure and evolution of biological solar power, Trends Biochem. Sci. 27 (2002) 79–87.
[51] X. Lin, H.A. Murchison, V. Nagarajan, W.W. Parson, J.P. Allen, J.C. Williams, Specific alteration of the oxidation potential of the electron donor in reaction centers from *Rhodobacter sphaeroides*, Proc. Natl. Acad. Sci. U. S. A. 91 (1994) 10265–10269.
[52] L. Kálmán, R. LoBrutto, J.P. Allen, J.C. Williams, Modified reaction centres oxidize tyrosine in reactions that mirror photosystem II, Nature 402 (1999) 696–699.
[53] A.J. Narváez, L. Kálmán, R. LoBrutto, J.P. Allen, J.C. Williams, Influence of the protein environment on the properties of a tyrosyl radical in reaction centers from *Rhodobacter sphaeroides*, Biochemistry 41 (2002) 15253–15258.
[54] R.J. Debus, Amino acid residues that modulate the properties of tyrosine Y_Z and the manganese cluster in the water oxidizing complex of photosystem II, Biochim. Biophys. Acta 1503 (2001) 164–186.
[55] D.E. Robertson, R.S. Farid, C.C. Moser, J.L. Urbauer, S.E. Mulholland, R. Pidikiti, J.D. Lear, A.J. Wand, W.F. DeGrado, P.L. Dutton, Design and synthesis of multi-haem proteins, Nature 368 (1994) 425–432.
[56] W.F. DeGrado, C.M. Summa, V. Pavone, F. Nastri, A. Lombardi, De novo design and structural characterization of proteins and metalloproteins, Annu. Rev. Biochem. 68 (1999) 779–819.
[57] A. Chakrabartty, R.L. Baldwin, Stability of α-helices, Adv. Protein Chem. 46 (1995) 141–176.
[58] D.N. Bolon, S.L. Mayo, Enzyme-like proteins by computational design, Proc. Natl. Acad. Sci. U. S. A. 98 (2001) 14274–14279.
[59] D.A. Moffet, M.H. Hecht, De novo proteins from combinatorial libraries, Chem. Rev. 101 (2001) 3191–3203.
[60] L. Balzter, H. Nilsson, J. Nilsson, De novo design of proteins—what are the rules?, Chem. Rev. 101 (2001) 3153–3163.
[61] B.R. Gibney, P.L. Dutton, De novo design and synthesis of heme proteins, Adv. Inorg. Chem. 51 (2001) 409–455.
[62] H.K. Rau, W. Haehnel, Design, synthesis, and properties of a novel cytochrome *b* model, J. Am. Chem. Soc. 120 (1998) 468–476.
[63] T. Kortemme, M. Ramírez-Alvarado, L. Serrano, Design of a 20-amino acid, three-stranded b-sheet protein, Science 281 (1998) 253–256.
[64] S.R. Griffiths-Jones, M.S. Searle, Structure, folding, and energetics of cooperative interactions between the β-strands of a de novo designed three-stranded antiparallel β-sheet peptide, J. Am. Chem. Soc. 122 (2000) 8350–8356.
[65] M.D. Struthers, R.P. Cheng, B. Imperiali, Design of a monomeric 23-residue polypeptide with defined tertiary structure, Science 271 (1996) 342–345.
[66] B.I. Dahiyat, S.L. Mayo, De novo design: fully automated sequence selection, Science 278 (1997) 82–87.
[67] R.S. Hodges, J. Sodek, L.B. Smillie, L. Jurasek, Tropomyosin: amino acid sequence and coiled-coil structure, Cold Spring Harbor Symp. Quant. Biol. 37 (1972) 299–310.
[68] R.S. Hodges, A.K. Saund, P.C.S. Chong, S.A. St.-Pierre, R.E. Reid, Synthetic model for two-stranded α-helical coiled-coils. Design, synthesis, and characterization of an 86-residue analog of tropomyosin, J. Biol. Chem. 256 (1981) 1214–1224.
[69] A.D. McLachlan, M. Stewart, Tropomyosin coiled-coil interactions: evidence for an unstaggered structure, J. Mol. Biol. 98 (1975) 293–304.
[70] S.Y.M. Lau, A.K. Taneja, R.S. Hodges, Synthesis of a model protein of defined secondary and quaternary structure. Effect of chain length on the stabilization and formation of two-stranded α-helical coiled-coils, J. Biol. Chem. 259 (1984) 13253–13261.
[71] N.L. Ogihara, M.S. Weiss, W.F. DeGrado, D. Eisenberg, The crystal structure of the designed trimeric coiled coil coil-V(a)L(d): implications for engineering crystals and supramolecular assemblies, Protein Sci. 6 (1997) 80–88.
[72] G.T. Dolphin, L. Brive, G. Johansson, L. Baltzer, Use of aromatic amino acid residues to restrict the dynamics in the hydrophobic core of a designed helix-loop-helix dimer, J. Am. Chem. Soc. 118 (1996) 11297–11298.
[73] B.R. Gibney, F. Rabanal, J.J. Skalicky, A.J. Wand, P.L. Dutton, Design of a unique protein scaffold for maquettes, J. Am. Chem. Soc. 119 (1997) 2323–2324.
[74] M.A. Willis, B. Bishop, L. Regan, A.T. Brunger, Dramatic structural and thermodynamic consequences of repacking a protein's hydrophobic core, Structure 8 (2000) 1319–1328.
[75] M.H. Hecht, J.S. Richardson, D.C. Richardson, R.C. Ogden, De novo design, expression, and characterization of Felix: a four-helix bundle protein of native-like sequence, Science 249 (1990) 884–891.
[76] R.B. Hill, W.F. DeGrado, Solutions structure of α_2D, a nativelike de novo designed protein, J. Am. Chem. Soc. 120 (1998) 1138–1145.
[77] J.J. Skalicky, B.R. Gibney, F. Rabanal, R.J. Bieber Urbauer, P.L. Dutton, A.J. Wand, Solution structure of a designed four-α-helix bundle maquette scaffold, J. Am. Chem. Soc. 121 (1999) 4941–4951.
[78] S.T.R. Walsh, H. Cheng, J.W. Bryson, H. Roder, W.F. DeGrado, Solution structure and dynamics of a de novo designed three-helix bundle protein, Proc. Natl. Acad. Sci. U. S. A. 96 (1999) 5486–5491.
[79] M.S. Searle, Peptide models of protein β-sheets: design, folding and insights into stabilising weak interactions, J. Chem. Soc., Perkin Trans. 2 (2001) 1011–1020.
[80] W. Wang, M.H. Hecht, Rationally designed mutations convert de novo amyloid-like fibrils into monomeric β-sheet proteins, Proc. Natl. Acad. Sci. U. S. A. 99 (2002) 2760–2765.
[81] R. Koradi, M. Billeter, K. Wüthrich, MOLMOL: a program for display and analysis of macromolecular structures, J. Mol. Graph. 14 (1996) 51–55.
[82] J.C. Ma, D.A. Dougherty, The cation-π interaction, Chem. Rev. 97 (1997) 1303–1324.
[83] J.P. Gallivan, D.A. Dougherty, Cation-π interactions in structural biology, Proc. Natl. Acad. Sci. U. S. A. 96 (1999) 9459–9464.

[84] H. Minoux, C. Chipot, Cation-π interactions in proteins: can simple models provide an accurate description?, J. Am. Chem. Soc. 121 (1999) 10366–10372.
[85] D.W. Banner, M. Kokkinidis, D. Tsemoglou, Structure of the ColE1 Rop protein at 1.7 Å resolution, J. Mol. Biol. 196 (1987) 657–675.
[86] P.J. Dillon, C.A. Rosen, Use of polymerase chain reaction for the rapid construction of synthetic genes, in: B.A. White (Ed.), PCR Protocols: Current Methods and Applications, Methods in Molecular Biology, vol. 15, Humana Press, Totowa, NJ, 1993, pp. 263–268.